10668 *Inorg. Chem.* **2010**, *49*, 10668–10679
DOI: 10.1021/ic1016752

Inorganic Chemistry
Article

Bioinorganic Chemistry of Parkinson's Disease: Structural Determinants for the Copper-Mediated Amyloid Formation of Alpha-Synuclein

Andrés Binolfi,[†] Esaú E. Rodriguez,[‡] Daniela Valensin,[§] Nicola D'Amelio,[∥] Emiliano Ippoliti,[⊥] Gonzalo Obal,[#] Rosario Duran,[#] Alessandra Magistrato,[⊥] Otto Pritsch,[#] Markus Zweckstetter,[▽,○] Gianni Valensin,[§] Paolo Carloni,[⊥] Liliana Quintanar,[‡] Christian Griesinger,[▽] and Claudio O. Fernández*[,†,▽]

[†]*Instituto de Biología Molecular y Celular de Rosario, Consejo Nacional de Investigaciones Científicas y Técnicas, Universidad Nacional de Rosario, Suipacha 531, S2002LRK, Rosario, Argentina,* [‡]*Departamento de Química, Centro de Investigación y de Estudios Avanzados* (*Cinvestav*), *Av. Instituto Politécnico Nacional 2508, 07360, D.F., México,* [§]*Dipartamento di Chimica, Universitá degli studi di Siena, Via Aldo Moro, 53100, Siena, Italy,* [∥]*Bracco Imaging-CRB Trieste, Area Science Park, Edificio Q, S. S., 14 Km, 163.5, 34149 Basovizza Trieste, Italy,* [⊥]*CNR-IOM-Democritos National Simulation Center and International School for Advanced Studies* (*SISSA/ISAS*), *via Beirut 2-4, I-34014 Trieste, Italy,* [#]*Institut Pasteur de Montevideo, Mataojo 2020, 11400 Montevideo, Uruguay,* [▽]*Department of NMR−based Structural Biology, Max Planck Institute for Biophysical Chemistry, Am Fassberg 11, D-37077 Göttingen, Germany, and* [○]*DFG Research Center for the Molecular Physiology of the Brain* (*CMPB*), *Göttingen, Germany*

Received August 18, 2010

The aggregation of alpha-synuclein (AS) is a critical step in the etiology of Parkinson's disease (PD). A central, unresolved question in the pathophysiology of PD relates to the role of AS-metal interactions in amyloid fibril formation and neurodegeneration. Our previous works established a hierarchy in alpha-synuclein-metal ion interactions, where Cu(II) binds specifically to the protein and triggers its aggregation under conditions that might be relevant for the development of PD. Two independent, non-interacting copper-binding sites were identified at the N-terminal region of AS, with significant difference in their affinities for the metal ion. In this work we have solved unknown details related to the structural binding specificity and aggregation enhancement mediated by Cu(II). The high-resolution structural characterization of the highest affinity N-terminus AS-Cu(II) complex is reported here. Through the measurement of AS aggregation kinetics we proved conclusively that the copper-enhanced AS amyloid formation is a direct consequence of the formation of the AS-Cu(II) complex at the highest affinity binding site. The kinetic behavior was not influenced by the His residue at position 50, arguing against an active role for this residue in the structural and biological events involved in the mechanism of copper-mediated AS aggregation. These new findings are central to elucidate the mechanism through which the metal ion participates in the fibrillization of AS and represent relevant progress in the understanding of the bionorganic chemistry of PD.

Introduction

Neurodegeneration in Parkinson's disease (PD) is characterized by the loss of dopaminergic neurons in the *substantia nigra pars compacta* and the presence of fibrillar cytoplasmic aggregates of the protein α-synuclein (AS) in multiple brain regions.[1−3] Evidence that AS amyloidogenesis plays a causative role in the development of PD is furnished by a variety of genetic, neuropathological, and biochemical studies.[3−6]

Structurally, AS comprises 140 amino acids distributed in three different regions: the amphipathic N-terminus (residues 1−60), showing the imperfect KTKEGV repeats and involved in lipid binding; the highly hydrophobic self-aggregating sequence that initiates fibrillation, known as NAC (residues 61−95);[7] and the acidic C-terminal region (residues

*To whom correspondence should be addressed. Phone: ++54 341 4448745. Fax: ++54 341 4390465. E-mail: fernandez@ibr.gov.ar or cfernan@gwdg.de.

(1) Forno, L. S. *J. Neuropathol. Exp. Neurol.* **1996**, *55*, 259–272.
(2) Spillantini, M. G.; Schmidt, M. L.; Lee, V. M.; Trojanowski, J. Q.; Jakes, R.; Goedert, M. *Nature* **1997**, *388*, 839–840.
(3) Goedert, M. *Nat. Rev. Neurosci.* **2001**, *2*, 492–501.
(4) Kruger, R.; Kuhn, W.; Muller, T.; Woitalla, D.; Graeber, M.; Kosel, S.; Przuntek, H.; Epplen, J. T.; Schols, L.; Riess, O. *Nat. Genet.* **1998**, *18*, 106–108.
(5) Volles, M. J.; Lansbury, P. T., Jr. *Biochemistry* **2003**, *42*, 7871–7878.
(6) Zarranz, J. J.; Alegre, J.; Gomez-Esteban, J. C.; Lezcano, E.; Ros, R.; Ampuero, I.; Vidal, L.; Hoenicka, J.; Rodriguez, O.; Atares, B.; Llorens, V.; Gomez Tortosa, E.; del Ser, T.; Munoz, D. G.; de Yebenes, J. G. *Ann. Neurol.* **2004**, *55*, 164–173.
(7) Giasson, B. I.; Murray, I. V.; Trojanowski, J. Q.; Lee, V. M. *J. Biol. Chem.* **2001**, *276*, 2380–2386.

 Published on Web 10/22/2010

96−140), rich in Pro, Asp, and Glu residues, and critical for blocking rapid AS filament assembly.[8,9] In its native monomeric state AS adopts an ensemble of conformations with no rigid secondary structure although long-range interactions have been shown to stabilize an aggregation-autoinhibited conformation.[10−13] The precise function of AS is unknown, as are the mechanism(s) underlying the structural transition from the innocuous monomeric conformations of AS to its neurotoxic forms.

There is now extensive evidence for the association of protein aggregation and neurodegeneration in many disorders.[14−19] Among the recent discoveries is the finding that protein aggregation and oxidative stress-induced damage represent a recurring phenomenon in all these pathologies.[20,21] Interestingly, metals such as copper, iron, and manganese appear to play an important role in protein aggregation and therefore are likely to provide a link between the two pathological processes of protein aggregation and oxidative damage.[21−23] Copper and manganese have been implicated in Creutzfeldt−Jakob disease. While Cu(II) has been shown to bind to the normal isoform of the prion protein, Mn(II) binding has been mainly associated with protein conversion into an abnormal isoform.[24,25] There is direct evidence that copper, iron, and zinc contribute to amyloid Aβ assembly in vitro and to the neuropathology of Alzheimer's disease.[26−28] High levels of copper, zinc, and iron were found in and around amyloid plaques of AD brains.[29] Furthermore, coordination environments for Cu(II) complexes in the amyloid precursor protein, the amyloid Aβ-peptide and the prion protein have been well characterized by several biophysical and structural studies.[30−37] The detailed knowledge of the structural and binding features of relevant metal ions, as well as the mechanism by which these metal ions may participate in the fibrillization of these proteins have contributed to the design of a new therapeutical scheme based in the development of metal ion chelators.[38]

Abnormal metal-protein interactions have also emerged as an important potential mechanism in the pathophysiological events in PD. Iron deposits have been identified in Lewy bodies in the *substantia nigra*,[39] and elevated copper concentrations have been reported in the cerebrospinal fluid of PD patients.[40] In addition, individuals with chronic industrial exposure to copper, manganese, or iron have an increased rate of PD,[41] whereas metal ions such as copper and iron have been shown to bind AS and accelerate its fibrillation in vitro.[42] The structural characterization of the interaction between AS and those metal ions strongly linked to the onset of PD has been recently explored by us and other groups.[43−50] A comparative analysis revealed a hierarchal effect of metal interactions on AS aggregation kinetics, dictated by structural factors corresponding to different protein domains.[45]

(8) Fernandez, C. O.; Hoyer, W.; Zweckstetter, M.; Jares-Erijman, E. A.; Subramaniam, V.; Griesinger, C.; Jovin, T. M. *EMBO J.* **2004**, *23*, 2039–2046.
(9) Hoyer, W.; Cherny, D.; Subramaniam, V.; Jovin, T. M. *Biochemistry* **2004**, *43*, 16233–16242.
(10) Bertoncini, C. W.; Jung, Y. S.; Fernandez, C. O.; Hoyer, W.; Griesinger, C.; Jovin, T. M.; Zweckstetter, M. *Proc. Natl. Acad. Sci. U.S.A.* **2005**, *102*, 1430–1435.
(11) Dedmon, M. M.; Lindorff-Larsen, K.; Christodoulou, J.; Vendruscolo, M.; Dobson, C. M. *J. Am. Chem. Soc.* **2005**, *127*, 476–477.
(12) Lee, J. C.; Gray, H. B.; Winkler, J. R. *J. Am. Chem. Soc.* **2005**, *127*, 16388–16389.
(13) Lee, J. C.; Lai, B. T.; Kozak, J. J.; Gray, H. B.; Winkler, J. R. *J. Phys. Chem. B* **2007**, *111*, 2107–2112.
(14) Baba, M.; Nakajo, S.; Tu, P. H.; Tomita, T.; Nakaya, K.; Lee, V. M.; Trojanowski, J. Q.; Iwatsubo, T. *Am. J. Pathol.* **1998**, *152*, 879–884.
(15) El-Agnaf, O. M.; Irvine, G. B. *Biochem. Soc. Trans.* **2002**, *30*, 559–565.
(16) Irvine, G. B.; El-Agnaf, O. M.; Shankar, G. M.; Walsh, D. M. *Mol. Med.* **2008**, *14*, 451–464.
(17) Lopes, D. H.; Colin, C.; Degaki, T. L.; de Sousa, A. C.; Vieira, M. N.; Sebollela, A.; Martinez, A. M.; Bloch, C., Jr.; Ferreira, S. T.; Sogayar, M. C. *J. Biol. Chem.* **2004**, *279*, 42803–42810.
(18) Masliah, E.; Rockenstein, E.; Veinbergs, I.; Mallory, M.; Hashimoto, M.; Takeda, A.; Sagara, Y.; Sisk, A.; Mucke, L. *Science* **2000**, *287*, 1265–1269.
(19) Spillantini, M. G.; Crowther, R. A.; Jakes, R.; Hasegawa, M.; Goedert, M. *Proc. Natl. Acad. Sci. U.S.A.* **1998**, *95*, 6469–6473.
(20) Allsop, D.; Mayes, J.; Moore, S.; Masad, A.; Tabner, B. J. *Biochem. Soc. Trans.* **2008**, *36*, 1293–1298.
(21) Requena, J. R.; Groth, D.; Legname, G.; Stadtman, E. R.; Prusiner, S. B.; Levine, R. L. *Proc. Natl. Acad. Sci. U.S.A.* **2001**, *98*, 7170–7175.
(22) Atwood, C. S.; Moir, R. D.; Huang, X. D.; Scarpa, R. C.; Bacarra, N. M. E.; Romano, D. M.; Hartshorn, M. K.; Tanzi, R. E.; Bush, A. I. *J. Biol. Chem.* **1998**, *273*, 12817–12826.
(23) Paik, S. R.; Shin, H. J.; Lee, J. H.; Chang, C. S.; Kim, J. *Biochem. J.* **1999**, *340*, 821–828.
(24) Brown, D. R.; Hafiz, F.; Glasssmith, L. L.; Wong, B. S.; Jones, I. M.; Clive, C.; Haswell, S. J. *EMBO J.* **2000**, *19*, 1180–1186.
(25) Kim, N. H.; Choi, J. K.; Jeong, B. H.; Kim, J. I.; Kwon, M. S.; Carp, R. I.; Kim, Y. S. *FASEB J.* **2005**, *19*, 783–785.
(26) Faller, P.; Hureau, C. *Dalton Trans.* **2009**, 1080–1094.
(27) Brown, D. R.; Kozlowski, H. *Dalton Trans.* **2004**, 1907–1917.
(28) Garzon-Rodriguez, W.; Yatsimirsky, A. K.; Glabe, C. G. *Bioorg. Med. Chem. Lett.* **1999**, *9*, 2243–2248.
(29) Lovell, M. A.; Robertson, J. D.; Teesdale, W. J.; Campbell, J. L.; Markesbery, W. R. *J. Neurol. Sci.* **1998**, *158*, 47–52.
(30) Guilloreau, L.; Damian, L.; Coppel, Y.; Mazarguil, H.; Winterhalter, M.; Faller, P. *J. Biol. Inorg. Chem.* **2006**, *11*, 1024–1038.
(31) Chattopadhyay, M.; Walter, E. D.; Newell, D. J.; Jackson, P. J.; Aronoff-Spencer, E.; Peisach, J.; Gerfen, G. J.; Bennett, B.; Antholine, W. E.; Millhauser, G. L. *J. Am. Chem. Soc.* **2005**, *127*, 12647–12656.
(32) Garnett, A. P.; Viles, J. H. *J. Biol. Chem.* **2003**, *278*, 6795–6802.
(33) Valensin, D.; Mancini, F. M.; Luczkowski, M.; Janicka, A.; Wisniewska, K.; Gaggelli, E.; Valensin, G.; Lankiewicz, L.; Kozlowski, H. *Dalton Trans.* **2004**, 16–22.
(34) Karr, J. W.; Szalai, V. A. *Biochemistry* **2008**, *47*, 5006–5016.
(35) Gaggelli, E.; Bernardi, F.; Molteni, E.; Pogni, R.; Valensin, D.; Valensin, G.; Remelli, M.; Luczkowski, M.; Kozlowski, H. *J. Am. Chem. Soc.* **2005**, *127*, 996–1006.
(36) Drew, S. C.; Masters, C. L.; Barnham, K. J. *J. Am. Chem. Soc.* **2009**, *131*, 8760–8761.
(37) Drew, S. C.; Noble, C. J.; Masters, C. L.; Hanson, G. R.; Barnham, K. J. *J. Am. Chem. Soc.* **2009**, *131*, 1195–1207.
(38) Gaeta, A.; Hider, R. C. *Br. J. Pharmacol.* **2005**, *146*, 1041–1059.
(39) Castellani, R. J.; Siedlak, S. L.; Perry, G.; Smith, M. A. *Acta Neuropathol.* **2000**, *100*, 111–114.
(40) Pall, H. S.; Blake, D. R.; Gutteridge, J. M.; Williams, A. C.; Lunec, J.; Hall, M.; Taylor, A. *Lancet* **1987**, *330*, 238–241.
(41) Gorell, J. M.; Johnson, C. C.; Rybicki, B. A.; Peterson, E. L.; Kortsha, G. X.; Brown, G. G.; Richardson, R. J. *Neurotoxicology* **1999**, *20*, 239–247.
(42) Uversky, V. N.; Li, J.; Fink, A. L. *J. Biol. Chem.* **2001**, *276*, 44284–44296.
(43) Rasia, R. M.; Bertoncini, C. W.; Marsh, D.; Hoyer, W.; Cherny, D.; Zweckstetter, M.; Griesinger, C.; Jovin, T.; Fernández, C. O. *Proc. Natl. Acad. Sci. U.S.A.* **2005**, *102*, 4294–4299.
(44) Binolfi, A.; Lamberto, G. R.; Duran, R.; Quintanar, L.; Bertoncini, C. W.; Souza, J. M.; Cervenansky, C.; Zweckstetter, M.; Griesinger, C.; Fernandez, C. O. *J. Am. Chem. Soc.* **2008**, *130*, 11801–11812.
(45) Binolfi, A.; Rasia, R. M.; Bertoncini, C. W.; Ceolin, M.; Zweckstetter, M.; Griesinger, C.; Jovin, T. M.; Fernandez, C. O. *J. Am. Chem. Soc.* **2006**, *128*, 9893–9901.
(46) Jackson, M. S.; Lee, J. C. *Inorg. Chem.* **2009**, *48*, 9303–9307.
(47) Lee, J. C.; Gray, H. B.; Winkler, J. R. *J. Am. Chem. Soc.* **2008**, *130*, 6898–6899.
(48) Wright, J. A.; Brown, D. R. *J. Neurosci. Res.* **2008**, *86*, 496–503.
(49) Drew, S. C.; Leong, S. L.; Pham, C. L.; Tew, D. J.; Masters, C. L.; Miles, L. A.; Cappai, R.; Barnham, K. J. *J. Am. Chem. Soc.* **2008**, *130*, 7766–7773.
(50) Lucas, H. R.; Lee, J. C. *J. Inorg. Biochem.* **2010**, *104*, 245–249.

From these studies it was shown that Cu(II) binds specifically to AS and is effective in accelerating aggregation at physiologically relevant concentrations.[43] Other divalent metal ions had a minimal or no stimulatory effect on AS fibrillation under these conditions.[45] Details of Cu(II) binding explored by matrix-assisted laser desorption/ionization mass spectroscopy (MALDI-MS) and NMR spectroscopy revealed the presence of two binding sites at the N-terminus, comprising the stretch of residues ^{1}MDVFMK^{6} and the His within the sequence ^{48}VAHGV^{52}.[43,44,51] The α-NH_2 nitrogen of Met-1 was identified as the metal anchoring group for the high affinity binding site ($K_{d1} = 0.2\ \mu M$).[44,46,47] Instead, the imidazol ring of His residue at position 50 in the N-terminal region represented a lower affinity binding motif for Cu(II) ($K_{d2} \approx 50\ \mu M$).[44] Despite the fact that Cu(II) binding at the N-terminal region is recognized as a key event triggering AS aggregation, the impact that these structural-affinity differences at the N-terminus might have on the aggregation process of AS has not been addressed to date.

In this work we sought to delineate the structural-aggregation basis behind the interaction of Cu(II) with the ^{1}MDVFMK^{6} sequence of AS, as a first step toward the understanding of the molecular mechanism by which Cu(II) accelerates AS filament assembly. The identity of the Cu(II) binding ligands and structural features of the high-affinity metal binding site were elucidated by the combined application of spectroscopic techniques and molecular dynamics. Through the design of site-directed mutants and synthetic peptide models of AS we demonstrated that Cu(II) binding to the high-affinity site is the critical step in the metal-mediated AS aggregation. This knowledge is central to understanding the structural and mechanistic basis behind the aggregation enhancement induced by Cu(II) on the fibrillization process of AS and sheds light onto the rational design of new therapeutic agents directed toward the treatment of neurodegeneration in PD.

Experimental Section

Proteins and Reagents. The proteins AS, H50A AS, 1−108 AS, and 1−108 H50A AS were prepared as previously described.[8,9] The H50A mutants were constructed using the Quick-Change site-directed mutagenesis kit (Stratagene) on AS sequence-containing plasmids. The introduced modifications were further verified by DNA sequencing. Purified proteins were dialyzed against Buffer A (20 mM MES, 20 mM MOPS, 100 mM NaCl, pH range 5.0−7.5) or Buffer B (20 mM Hepes, 100 mM NaCl, pH 7.5), all treated with Chelex (Sigma). Peptides ^{1}MDVFMK^{6} (P1AS) and ^{1}MAVFMK^{6} (D2A-P1AS) were synthesized in solid-phase (Rink amide resin) using F-moc chemistry in a peptide synthesizer (CEM Liberty). They were purified by reverse phase HPLC (Waters Delta 600) and characterized by HPLC and electrospray ionization mass spectrometry (Agilent). Both peptides were amidated at the C-terminal carboxylate group, while the α-NH_2 terminal was left unmodified. The concentrations of P1AS and D2A-P1AS solutions were determined by weighing out dry peptide samples. Peptide methylation reagent was prepared by dropwise addition of acetyl chloride to anhydrous methanol as previously described.[52] Peptide methylation reactions were performed at room temperature for 1 h. Peptide modification with diethyl pyrocarbonate (DEPC) was performed by reacting the peptide with a 5-fold molar excess of DEPC (Sigma) at room temperature for 30 min. In some experiments, prior to DEPC modification, samples were incubated with a 10-fold molar excess of $CuSO_4$ at room temperature for 30 min. $CuSO_4$ salt of the highest purity available was purchased from Merck. Deuterium oxide, sodium deuteroxide, and d_3-glycerol were purchased from Sigma, while deuterated MES buffer and 60−70% ^{17}O enriched water were purchased from Cambridge Isotope Laboratories.

Isothermal Titration Calorimetry (ITC). ITC measurements were performed using a VP-ITC instrument (MicroCal). Peptide and protein samples were dissolved in buffer B. In the experimental setup, the cell was filled with peptide or protein samples, and the syringe was filled with the metal ion solutions. Experiments were performed with 28 injections of 10 μL, duration of 10 s, and spacing of 180 s. A background titration of the buffer solution in the sample cell with an identical metal ion solution was subtracted from each experimental titration to account for the heat of dilution. To determine the affinity features of the AS-Cu(II) complex, the MicroCal ORIGIN software package was used to simultaneously fit the data to a model incorporating complexes of Cu(II) in one binding site or in two classes of independent, non-interactive binding sites.

Electronic Absorption and CD Spectroscopy. Electronic absorption spectra in the UV−visible region were collected on a Jasco V-550 spectrophotometer. CD spectra were acquired with a Jasco J-800 spectrapolarimeter. Cu(II) titration experiments were performed at 15 °C on samples containing 300 μM peptide or protein in buffer A. Data were expressed as difference absorbance (ε) or circular dichroism (Δε) per molar concentration of protein.

EPR Spectroscopy. Protein and peptide samples for electron paramagnetic resonance (EPR) were prepared in buffer A with 50% glycerol to achieve adequate glassing. Peptide or protein concentrations were in the order of 500 to 700 μM. X-band EPR spectra were collected using either a Bruker ELEXSYS E500 system or a Bruker EMX spectrometer with an ER 041 XG microwave bridge and ER 4102ST cavity. EPR spectra were collected either at 77 K using a finger dewar with liquid nitrogen or at 150 K using a ER4131VT variable temperature nitrogen system. The following conditions were used: microwave frequency, 9.4 GHz; microwave power, 10 mW; modulation amplitude, 5 G; modulation frequency, 100 kHz; time constant, 327 ms; conversion time, 82 ms; and averaging over 12 scans. EPR spectra were baseline-corrected and simulated using the programs WinEPR SimFonia and XSophe (Bruker).[53] For experiments performed in ^{17}O water, the peptide P1AS was dissolved in buffer A, pH 6.5, prepared with 60−70% enriched $H_2{}^{17}O$ (Cambridge Isotope Laboratories) and 30% glycerol to achieve adequate glassing. The pH of the final solution was adjusted using a microelectrode and a solution of NaOH in 60−70% enriched $H_2{}^{17}O$. Final P1AS concentration was 850 μM and 0.8 equiv of Cu(II) were added. A P1AS sample in ^{16}O water was prepared in parallel using the same protocol for each experiment. X-Band EPR spectra of these samples were collected using a Bruker EMX Plus system with an ER4112HV continuous flow liquid helium cryostat. Conditions: microwave frequency: 9.4 GHz; temperature 20 K, microwave power 1 mW, modulation amplitude, 5 G; modulation frequency, 100 kHz; time constant, 327 ms; conversion time, 82 ms; and averaging over 12 scans.

MALDI-TOF Mass Spectrometry. Peptide samples were desalted using C18 reverse phase microcolumns (OMIX Pipette tips, Varian) and eluted directly into the mass spectrometer sample plate with 2 μL of matrix solution (α-cyano-4-hydroxycinnamic acid in 60% aqueous acetonitrile containing 0.2%

(51) Sung, Y. H.; Rospigliosi, C.; Eliezer, D. *Biochim. Biophys. Acta* **2006**, *1764*, 5–12.
(52) Ficarro, S.; Chertihin, O.; Westbrook, V. A.; White, F.; Jayes, F.; Kalab, P.; Marto, J. A.; Shabanowitz, J.; Herr, J. C.; Hunt, D. F.; Visconti, P. E. *J. Biol. Chem.* **2003**, *278*, 11579–11589.
(53) Hanson, G. R.; Gates, K. E.; Noble, C. J.; Griffin, M.; Mitchell, A.; Benson, S. *J. Inorg. Biochem.* **2004**, *98*, 903–916.

trifluoroacetic acid). Molecular masses of native and modified peptides were determined in a 4800 MALDI TOF/TOF instrument (Applied Biosystems) using α-cyano-4-hydroxycinnamic acid as the matrix. External calibration was performed with a mixture of peptide standards (Applied Biosystems). For the identification of modified residues, collision-induced dissociation (CID) MS/MS experiments were performed.

NMR Spectroscopy. NMR spectra were acquired on a Bruker Avance II 600 MHz spectrometer using a triple-resonance probe equipped with *z*-axis self-shielded gradient coils. The NMR experiments were performed on 600 μM (^{1}H NMR) or 2.5 mM (^{13}C NMR) peptide samples dissolved in water, deuterium oxide, or deuterated Buffer A in the range 15−25 °C. Proton and carbon resonances were assigned by ^{1}H-^{1}H TOCSY (16 scans), ^{1}H-^{1}H NOESY (32 scans), ^{1}H-^{13}C HSQC (128 scans) and ^{1}H-^{13}C HMBC (512 scans) experiments. Chemical shifts were referenced to DSS as internal standard. ^{1}H-^{1}H TOCSY, ^{1}H-^{13}C HSQC, and ^{1}H-^{13}C HMBC cross peaks affected during titrations with Cu(II) were identified by comparing their intensities (I) with those of the same cross peaks (I_0) in the data set of samples lacking Cu(II).

Proton spin−lattice relaxation rates were measured with the standard inversion recovery (IR) pulse sequence; relaxation rates were calculated with regression analysis of the initial recovery curves of longitudinal magnetization components, leading to errors in the ±3%. While the simple IR experiment is suitable for the well-isolated peaks, the IR-TOCSY sequence was used to calculate the relaxation rates of the overlapping ^{1}H NMR signals.[35,54] The T_1 values were determined by a three-parameter fit of peak intensities to the following equation:

$$I(t) = I_0[1 - (1 + B)\exp(-t/T_1)] \quad (1)$$

where B is a variable parameter that considers non-ideal magnetization whose value is less than unity. The results were compared with those obtained from the normal IR sequence. The agreement was found within the errors limit of both experiments.

The paramagnetic contributions of Cu(II) to the spin−lattice relaxation rate, R_{1p}, were calculated according to[55]

$$R_{1p} = R_{1obs} - p_f R_{1free} = \frac{p_b}{R_{1b}{}^{-1} + \tau_M} \quad (2)$$

where f and b refer to the free and metal-bound states, respectively, the $p's$ are fractional populations of the peptide, R_{1free} and R_{1b} are the spin−lattice relaxation rates in the two environments, and τ_M (the inverse of the off-rate kinetic constant) is the residence time of the peptide in the metal coordination sphere. R_{1b} ($1/T_{1b}$) is accounted for by the Solomon equation describing the dipole−dipole nuclear spin-electron spin interaction, here reported for systems with $S = 1/2$:[56]

$$R_{1b} = \frac{1}{10}\left(\frac{\mu_0}{4\pi}\right)^2 \frac{\hbar^2 \gamma_I{}^2 \gamma_S{}^2}{r^6}\left\{\frac{\tau_C}{1 + (\omega_I - \omega_S)^2\tau_C{}^2} + \frac{3\tau_C}{1 + \omega_I{}^2\tau_C{}^2} + \frac{6\tau_C}{1 + (\omega_I - \omega_S)^2\tau_C{}^2}\right\} \quad (3)$$

where μ_o is the permeability of vacuum, γ_I and γ_S are the nuclear and electron magnetogyric ratios, respectively, $\hbar$ is the reduced Planck constant, ω_I and ω_S are the nuclear and electron Larmor frequencies, respectively, r is the proton−metal distance, and τ_c is the effective correlation time.

Acquisition, processing and visualization of the NMR spectra were performed using TOPSPIN 2.0 (Bruker) and Sparky.

Classical MD and QM/MM Simulations. Eighteen representative structures covering about 50% of the conformational space spanned by the NMR data on the protein in solution were used to construct the adducts with copper.[10,11,57] The metal ion was imposed to bind to the N-terminal Met-1 and Asp-2 backbone nitrogens, Asp-2 carboxylate side-chain, and a water molecule. The systems were neutralized by adding Na^+ counterions and immersed in water. Depending on the representative structure, the systems ranged from ∼30,000 to 80,000 atoms. The protein atoms and counterions were represented by parameters from the Amber ff99 force field, supplemented by TIP3P water molecules.[58,59] The parametrization procedure for the copper coordination sphere is described in the Supporting Information. Each system was subjected to 10 ns classical molecular dynamics (MD) simulations at 300 K and 1 atm pressure, by using the "weak coupling" Berendsen thermostat and isotropic position scaling barostat.[60]

The last snapshot of the classical MD simulation of each conformer was used as starting structure for quantum/classical (QM/MM) MD simulations at 300 K.[61] A 4 ps long simulation for each conformer was performed. The Car−Parrinello molecular dynamics program (CPMD) was used for the QM/MM simulations.[62] The method relies on density functional theory (DFT) to solve the quantum problem and employs the AMBER force field for the MM part. The QM part (27 atoms) consisted of Cu(II), the N-terminal Met-1 backbone unit and its side-chain up to the C_β atom, the entire Asp-2 residue, and a water molecule coordinating the copper ion. Capping hydrogen atoms were added to the QM region to saturate valences of terminal carbon atoms. To avoid affecting the electronic structure of the QM part by the spurious interactions between such capping hydrogens and the close-by classical atoms, the fictitious electrostatic interactions between the QM capping hydrogens and the classical atoms within 2 Å were excluded as previously described.[63]

The time step for the dynamics was 0.1 fs, and the fictitious electronic mass was chosen to be 600 au. An energy cutoff of 70 Ry and gradient corrected PBE exchange-correlation functional were used.[64] The core−valence electron interactions for the C, N, O, and H atoms were described using non-conserving Martins and Troullier pseudopotentials, corrected for a better description of van der Waals interactions.[65,66] The employed Cu(II) pseudopotential corresponded to that successfully used for other biological applications.[67] Integration of the nonlocal parts of the pseudopotential was obtained via the Kleinman−Bylander scheme for all atoms except for Cu(II), for which a Gauss−Hermite numerical integration scheme was used.[68] Electrostatic interactions between periodic images of the QM part were decoupled by a previously described scheme,[69] while those of the classical part with periodic

(54) Huber, J. G.; Moulis, J. M.; Gaillard, J. *Biochemistry* **1996**, *35*, 12705–12711.
(55) Bertini, I.; Luchinat, C. *Coord. Chem. Rev.* **1996**, *150*, 1–296.
(56) Solomon, I. *Phys. Rev.* **1955**, *99*, 559–565.
(57) Herrera, F. E.; Chesi, A.; Paleologou, K. E.; Schmid, A.; Munoz, A.; Vendruscolo, M.; Gustincich, S.; Lashuel, H. A.; Carloni, P. *PloS One* **2008**, *3*, e3394.
(58) Jorgensen, W. L.; Chandrasekhar, J.; Madura, J. D.; Impey, R. W.; Klein, M. L. *J. Phys. Chem.* **1983**, *79*, 926–935.
(59) Wang, J.; Cieplak, P.; Kollman, P. A. *J. Comput. Chem.* **2000**, *21*, 1049–1074.
(60) Berendsen, H. C. J.; Postma, J. P. M.; van Gunsteren, W. F.; DiNola, A.; Haak, J. R. *J. Chem. Phys.* **1984**, *81*, 3684–3690.
(61) Laio, A.; VandeVondele, J.; Rothlisberger, U. *J. Chem. Phys.* **2002**, *116*, 6941–6948.
(62) CPMD Consortium (2006) CPMD 3.11.1; (Max-Planck-Institut für Festkörperforschung and IBM Zurich Research Laboratory); www.cpmd.org.
(63) Laio, A.; Gervasio, F. L.; VandeVondele, J.; Sulpizi, M.; Rothlisberger, U. *J. Phys. Chem. B* **2004**, *108*, 7963–7968.
(64) Perdew, J. P.; Burke, K.; Ernzerhof, M. *Phys. Rev. Lett.* **1996**, *77*, 3865–3868.
(65) Troullier, N.; Martins, J. L. *Phys. Rev. B* **1991**, *43*, 1943–2006.
(66) von Lilienfeld, O. A.; Tavernelli, I.; Rothlisberger, U.; Sebastiani, D. *Phys. Rev. Lett.* **2004**, *93*, 153004–153008.
(67) Cascella, M.; Magistrato, A.; Tavernelli, I.; Carloni, P.; Rothlisberger, U. *Proc. Natl. Acad. Sci. U.S.A.* **2006**, *103*, 19641–19646.
(68) Kleinman, L.; Bylander, D. M. *Phys. Rev. Lett.* **1982**, *18*, 1425–1428.
(69) Martyna, G. J.; Tuckerman, M. E. *J. Chem. Phys.* **1999**, *110*, 2810–2821.

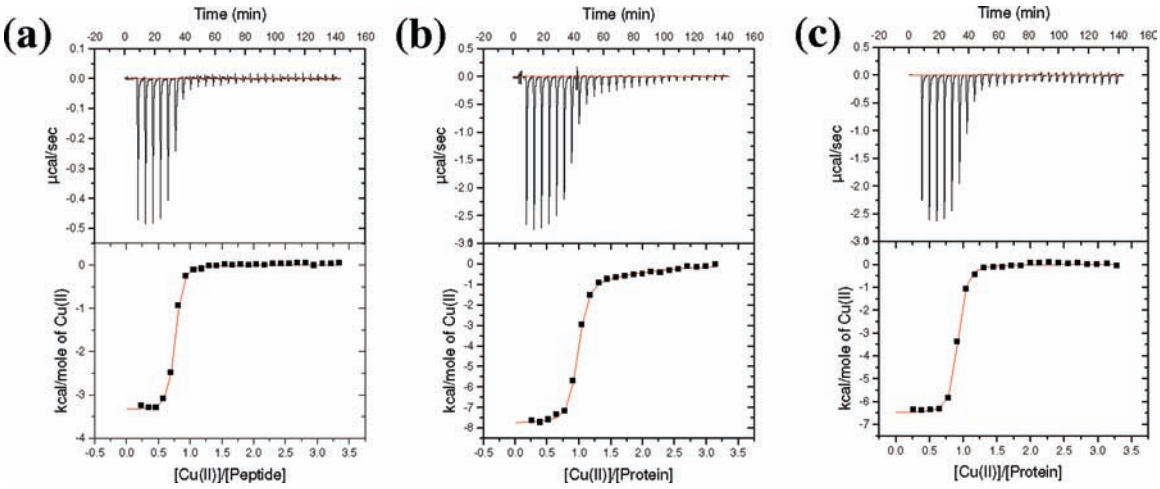

Figure 1. ITC of Cu(II) titration experiments performed on 30 μM P1AS peptide (a), 70 μM WT AS (b), and 70 μM H50A AS samples (c). The points in the titration curves (■) correspond to the integral of each signal, whereas red lines are the fittings to the selected models. The following parameters were estimated from (a) $K_{d1} = 0.11 \pm 0.01$ μM ($\Delta H_1 = -3346 \pm 25$ cal/mol, $\Delta S_1 = 20$ cal/mol °C); (b) $K_{d1} = 0.11 \pm 0.01$ μM ($\Delta H_1 = -7768 \pm 48$ cal/mol, $\Delta S_1 = 5$ cal/mol °C), $K_{d2} = 35.0 \pm 4.0$ μM ($\Delta H_2 = -1142 \pm 178$ cal/mol, $\Delta S_2 = 17$ cal/mol °C); and (c) $K_{d1} = 0.12 \pm 0.01$ μM ($\Delta H_1 = -6401$ cal/mol, $\Delta S_1 = 9$ cal/mol °C). In all cases, experiments were carried out in buffer B, pH 7.5, at 15 °C.

boundary conditions were treated by the particle−particle, particle-mesh method. A Nosé-Hoover thermostat was used to maintain a constant temperature.[70,71]

Aggregation Assays. Aggregation kinetics measurements were performed with 100 μM protein samples dissolved in buffer A. Samples were incubated at 37 °C under constant stirring. The amount of soluble AS monomers at different time points of the aggregation assay were determined by integration of the protein NMR resonances in the aliphatic region of the 1D ^{1}H NMR spectrum (0.4−2.1 ppm). Aggregation yields were normalized to the final values, and the averaged data points were fitted as previously described.[8,45] In all cases, the reported values correspond to the average of at least three independent aggregation measurements.

Results and Discussion

Cu(II) Affinity Features of P1AS Peptide. To determine whether the synthetic peptide P1AS, containing the sequence ^{1}MDVFMK^6, could be a useful model for elucidating structural details of Cu(II) binding to the high-affinity site of AS (hereafter referred to as site 1) we investigated the affinity features of Cu(II) binding to P1AS by isothermal titration calorimetry (ITC). To perform a comparative analysis, AS and its H50A mutant were also studied using this technique.

Figure 1 shows ITC measurements of the P1AS, WT AS, and H50A AS species titrated with Cu(II). As expected, P1AS and H50A AS data fit to a model that assumed binding of 1 equiv of Cu(II) per molecule (with dissociation constant K_{d1}), whereas a model incorporating complexes of Cu(II) in two classes of independent, non-interactive binding sites (K_{d1} and K_{d2}) had to be considered for the WT AS species.[44] From these experiments, we estimated the following values: $K_{d1} = 0.11 \pm 0.01$ μM for the PIAS-Cu(II) complex, $K_{d1} = 0.12 \pm 0.01$ μM for the H50 AS-Cu(II) complex, and $K_{d1} = 0.11 \pm 0.01$ μM/$K_{d2} = 35.0 \pm 4.0$ μM for the WT AS copper complexes.

The results shown here confirm previous findings,[44,46,47] indicating that (i) the free amino group at the N-terminus of AS is involved in the high-affinity site for Cu(II) binding to the protein; (ii) the Cu(II) binding motifs at the N-terminal region constitute separate, independent metal binding sites, and (iii) the transient long-range interactions in AS do not influence the binding preferences of Cu(II) at each site. Our data also indicates that the affinity features of the high affinity binding site in the full length protein are preserved in the P1AS species.

Coordination Properties of the P1AS-Cu(II) Complex. Cu(II) binding to site 1 was monitored by visible electronic absorption, Circular Dichroism (CD), and Electron Paramagnetic Resonance (EPR) spectroscopy upon titrations of P1AS with increasing concentrations of added Cu(II). To perform a comparative analysis, the variant H50A of AS was also studied by these techniques.

At substoichiometric Cu(II)/P1AS ratios, the UV−vis absorption spectrum of the P1AS-Cu(II) complex in buffer A at pH 6.5 is characterized by a single visible absorption band at 610 nm, that saturated after 1 equiv of Cu(II) was added, with $\varepsilon = 64$ M^{-1} cm^{-1}, typical of a Cu(II) d-d transition (Figure 2a). The absorption maximum (λ_{max}) is sensitive to the identity of the metal ligands and can be used as an indication of the number of nitrogen ligands bound to the Cu(II) ion.[72] The visible absorption spectrum of the P1AS-Cu(II) complex is characteristic of two- or three-nitrogen coordination in a type 2 square-planar or distorted tetragonal arrangement.

The CD spectrum of P1AS complexed with 1 equiv of Cu(II) in buffer A at pH 6.5 is characterized by the presence of a positive d-d band at 610 nm ($\Delta\varepsilon = 0.22$ M^{-1} cm^{-1}) and a negative charge transfer (CT) band at 300 nm ($\Delta\varepsilon = -1.1$ M^{-1} cm^{-1}) (Figure 2b). The intense band at 300 nm corresponds well with a ligand to metal CT transition originated from a deprotonated peptide amide [(N$^-$)−Cu CT, 295−315 nm],[73] supporting the involvement of a deprotonated

(70) Hoover, W. G. *Phys. Rev. A* **1985**, *31*, 1695–1697.
(71) Nose, S. J. *J. Chem. Phys.* **1984**, *81*, 511–519.
(72) Sigel, H.; Martin, R. B. *Chem. Rev.* **1982**, *82*, 385–426.
(73) Daniele, P. G.; Prenesti, E.; Ostacoli, G. *J. Chem. Soc., Dalton Trans.* **1996**, 3269–3275.

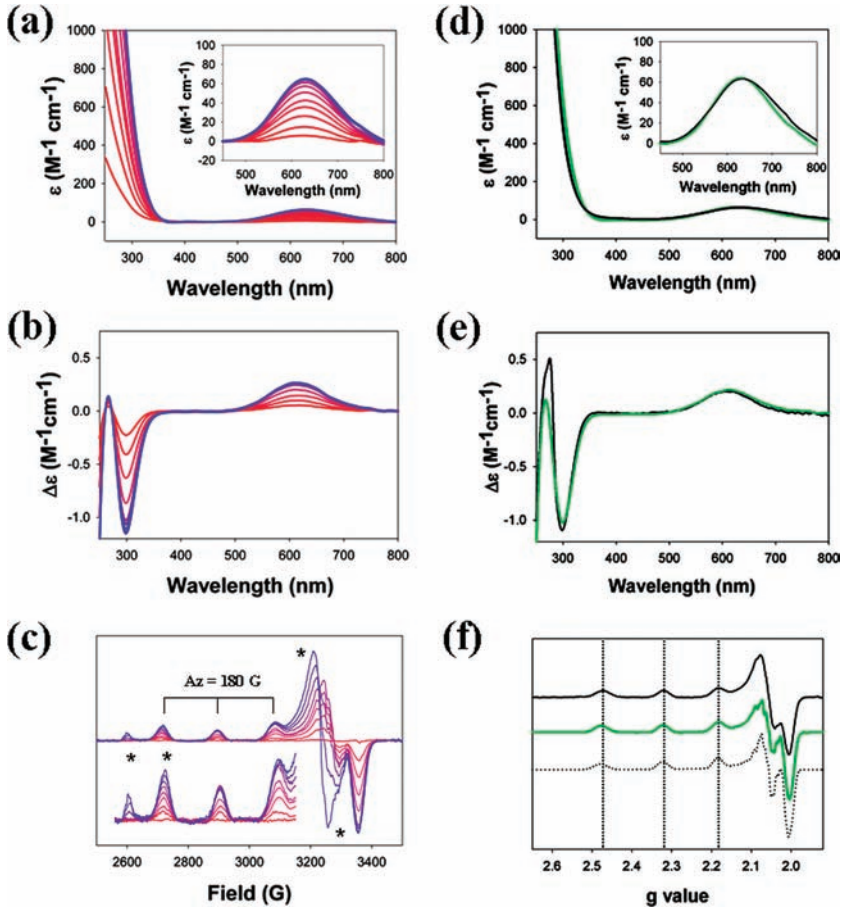

Figure 2. UV−vis absorption, CD, and EPR spectra of the high-affinity AS-Cu(II) complex. Direct titration of P1AS with Cu(II) monitored by absorption (a), CD (b), and X-band EPR (c) spectroscopy. Metal ion concentration was incremented by 0.1 equiv in (a), 0.2 equiv in (b), and 0.25 equiv in (c) until 2 equiv of Cu(II) added (in all cases, from red to blue). Asterisks in (c) indicate the EPR signals corresponding to free Cu(II) in solution. Overlaid absorption (d) and CD (e) spectra of P1AS (green line) and H50A AS (black line) with 1 equiv of Cu(II) added. X-band EPR spectra of P1AS (green) and H50A AS (black) with 1 equiv of Cu(II) added are shown in panel f. Dotted line in (f) corresponds to the EPR simulation of the experimental spectrum of the P1AS species. Enlargements of the transition region in the UV−vis spectra (a and d) and of the parallel region of the EPR spectra (c) are shown as insets. Spectra were collected in buffer A at pH 6.5 and 15 °C, under the conditions specified in the Experimental Section.

backbone amide nitrogen in the coordination of Cu(II) to site 1. No additional bands or wavelength shifts are detected in the CD spectrum beyond 1 equiv of Cu(II), consistent with the formation of a 1:1 P1AS-Cu(II) complex.

The titration of P1AS with Cu(II) followed by X-band EPR at pH 6.5 is shown in Figure 2c. The EPR signal that grows in upon addition of Cu(II) is characteristic of a type-2 copper site, with $g_z > g_{x,y} > 2.0$ and a large parallel hyperfine splitting (A_z), indicative of a $d_{x^2-y^2}$ ground state, as reported for the AS and BS high-affinity site.[43,44,49] After 1 equiv of Cu(II) was added, the EPR signal of the P1AS-Cu(II) complex saturates, and a second signal appears (indicated by asterisks in Figure 2c), which corresponds to free Cu(II) in solution. The g_z and A_z values associated to the P1AS-Cu(II) complex ($g_z = 2.25$ and $A_z = 180$ G $\equiv 189 \times 10^{-4}$ cm^{-1}) are indicative of an N2O2 equatorial coordination environment.[74,75] The EPR simulation of the experimental spectrum is shown in Figure 2f (dotted line), and it was obtained using the parameters listed in Table S1 in the Supporting Information. The superhyperfine structure from nitrogen in the perpendicular region of the spectrum can be simulated considering the superhyperfine interaction of two non-equivalent nitrogens with the electron spin. Our previous findings showing the involvement of the N-terminal α-NH_2 group of AS in copper binding and the presence of a CT band in the CD spectra of P1AS-Cu(II) complex (Figure 2b), assigned to the interaction between the metal ion and a deprotonated amide group, gives further support to this hypothesis.[44]

The results shown here indicate that the spectroscopic features of the P1AS-Cu(II) complex are identical to those recorded for the high-affinity binding site in WT AS[43,44] and mutant H50A AS (Figures 2 d−f), confirming that the electronic structure of the Cu(II) binding site 1 is preserved in the P1AS peptide. Overall, the affinity and spectroscopic data shown here indicate that the P1AS species constitutes an excellent model for addressing unresolved structural details of Cu(II) binding to site 1 in the full length protein.

To gain further insights into the structural features of Cu (II) binding to site 1, we also monitored the effect of pH on the P1AS-Cu(II) complex by CD and UV−vis spectroscopy (Figures 3 a,b). Complete loss of metal binding was observed below pH 4.0, as reflected by the disappearance of the visible electronic absorption and CD bands. As the pH is raised from 4.0 to 5.5 the

(74) Peisach, J.; Blumberg, W. E. *Arch. Biochem. Biophys.* **1974**, *165*, 691–708.
(75) Sakaguchi, U. A.; W., A. *J. Chem. Soc., Dalton Trans.* **1979**, 600–608.

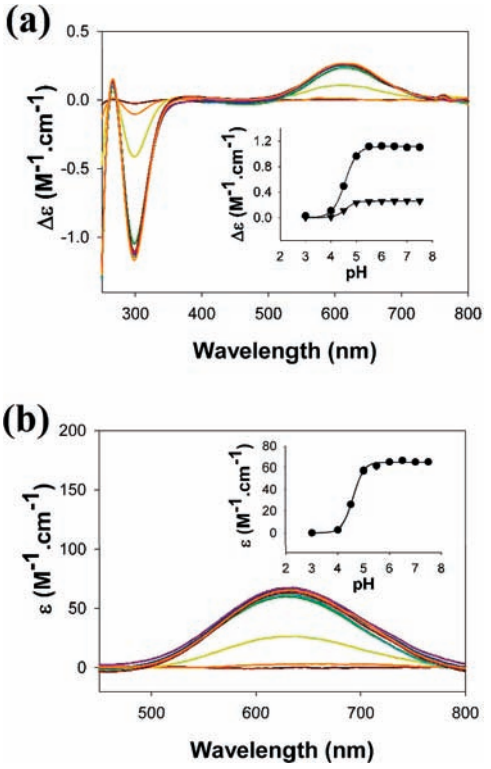

Figure 3. pH dependence of Cu(II) binding to P1AS. (a) CD spectra of P1AS with 1 equiv of Cu(II) in the 3.0−7.5 pH range. Inset shows $\Delta\varepsilon$ values (M^{-1} cm^{-1}) at 610 nm (▼) and 300 nm (●) at each pH value and the corresponding sigmoidal fittings of the data points (solid lines). (b) UV−vis spectra (ligand-field region) of P1AS with 1 equiv of Cu(II) in the 3.0−7.5 pH range. Inset shows the ε values (M^{-1} cm^{-1}) at 610 nm (●) at each pH value and the corresponding sigmoidal fittings of the data points (solid lines). Color lines in (a) and (b) correspond to the following pH values: 3.0 (brown), 4.0 (orange), 4.5 (yellow), 5.0 (green), 5.5 (cyan), 6.0 (blue), 6.5 (magenta), 7.0 (light brown), 7.5 (light orange). Spectra were collected in buffer A at 15 °C, under the conditions specified in the Experimental Section.

absorption increases in intensity, but it shows no wavelength shift, while no changes in the spectral features are observed in the pH range 5.5−7.5. The pH titration curve is consistent with a pK_a value of 4.6 (insets, Figures 3 a,b).

The effect of pH on the P1AS-Cu(II) complex was also monitored by EPR. Figure S1 in the Supporting Information shows the EPR spectra of the complex in the pH range 5.0−7.5. While the EPR spectra of the complex in the pH range 6.0−7.5 are identical, the EPR intensity is slightly decreased, and a second set of signals corresponding to free Cu(II) in solution become evident at pH 5.0, consistent with a lower complex population at this pH value.

Role of Asp-2 in Cu(II) Binding Site 1. The spectroscopic analysis of Cu(II) binding to P1AS revealed a square-planar or distorted tetragonal geometry with an N2O2 ligand donor set. We have demonstrated recently that the N-terminal α-NH_2 group of Met-1 in the ^{1}MDVFMK^6 sequence acts as an anchoring point for copper.[44] It is known that when the metal binds to the terminal amino group it favors the deprotonation of the amide group of the second residue.[72,76] The involvement of a deprotonated amide nitrogen in Cu(II) coordination to the site 1 of AS is supported by the presence of the CT band in the CD spectra of the P1AS-Cu(II) complex (~300 nm), whereas the pK_a value of the P1AS-Cu(II) complex demonstrates that the Asp at position 2 is the source of that nitrogen.[76,77] However, no direct clues have been reported regarding to the identity of the residues providing the oxygen ligands.

The Asp residue in position 2 of AS has been proposed as a potential source for the establishment of a Cu−O binding mode.[77] Indeed, model peptides with aspartyl residues in position 2 were shown to form highly stable Cu(II) complexes through direct Cu(II) coordination to the α-NH_2 group of residue 1 and deprotonated amide nitrogen and carboxylate side chains of residue at position 2. The high stability of the (α-NH_2, N^-, β-COO^-)-Cu(II) coordination environment was attributed to the presence of an extra negative charge and the formation of (5,6)-membered joined chelate rings.[76] These evidence prompted us to investigate the direct role of Asp-2 in Cu(II) binding site 1 of AS.

A mass spectrometry approach based on the selective modification of Asp-2 in the peptide P1AS was used first. The peptide P1AS was reacted with methanolic acetyl chloride to perform the selective methylation of the carboxylate side-chain of the Asp-2 residue prior to MALDI-MS analysis. The monoisotropic molecular mass [MH+] determined for the P1AS species is 769.37 Da (Figure S2a in the Supporting Information). After the methylation reaction, a major species was detected at m/z 783.39 (Figure S2b in the Supporting Information). On the basis of a predicted mass shift of 14.02 Da per each incorporated methyl group, this signal was assigned to the monomethylated species of P1AS (met-P1AS). No other modified species were detected, except by the presence of a small fraction of unmodified peptide. Collision induced dissociation MS/MS experiments identified Asp-2 as the methyl-modified residue in the P1AS sequence (Figures S2 c and d and Table S2 in the Supporting Information).

To ascertain the Cu(II) binding capability of the met-P1AS species, we performed experiments based on the protection from DEPC modification. Briefly, DEPC is a chemical that is capable of reacting with copper anchoring sites (i.e., imidazol ring and α-amino groups) to produce N-carbetoxy derivatives with a mass shift of 72.06 Da, whereas metal coordination to peptides or proteins are expected to protect the involved amino acids from DEPC modification.[44,78] We have successfully used this approach before to identify the location of Cu(II) anchoring residues in AS and beta-synuclein (BS).[44] Figure 4 shows the mass spectra of untreated (a), DEPC-treated (b), and Cu(II)-preincubated and DEPC-treated (c) met-P1AS samples. As mentioned above, the monomethylated peptide (met-P1AS) was detected at m/z 783.39 in the mass spectrum of DEPC-untreated samples, while this peak disappeared in the mass spectrum of the DEPC-treated met-P1AS, to be replaced with a new peak at m/z 855.43, corresponding to monocarbethoxylation of met-P1AS. Interestingly, preincubation with Cu(II)

(76) Kallay, C.; Varnagy, K.; Micera, G.; Sanna, D.; Sovago, I. *J. Inorg. Biochem.* **2005**, *99*, 1514–1525.

(77) Kowalik-Jankowska, T.; Rajewska, A.; Wisniewska, K.; Grzonka, Z.; Jezierska, J. *J. Inorg. Biochem.* **2005**, *99*, 2282–2291.

(78) Qin, K.; Yang, Y.; Mastrangelo, P.; Westaway, D. *J. Biol. Chem.* **2002**, *277*, 1981–1990.

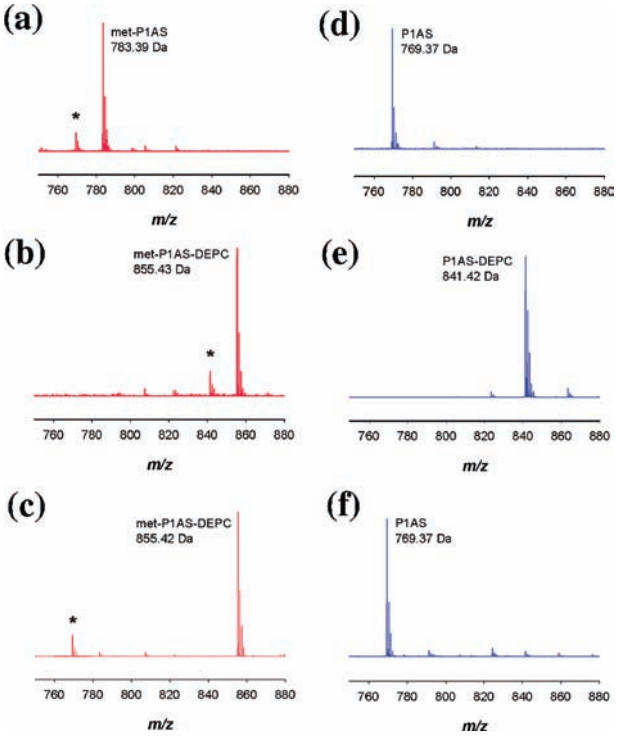

Figure 4. Effects of Cu(II) on DEPC modifications of the met-P1AS and P1AS peptides. MALDI-MS spectra of untreated (a), DEPC-modified (b), and Cu(II)-incubated and DEPC-modified (c) met-P1AS. Asterisks indicate a small population of unmethylated peptide. For comparative purposes MALDI-MS spectra of untreated (d), DEPC-modified (e) and Cu(II)-incubated and DEPC-modified (f) P1AS were obtained. Spectra were recorded at 25 °C, under the conditions specified in the Experimental Section.

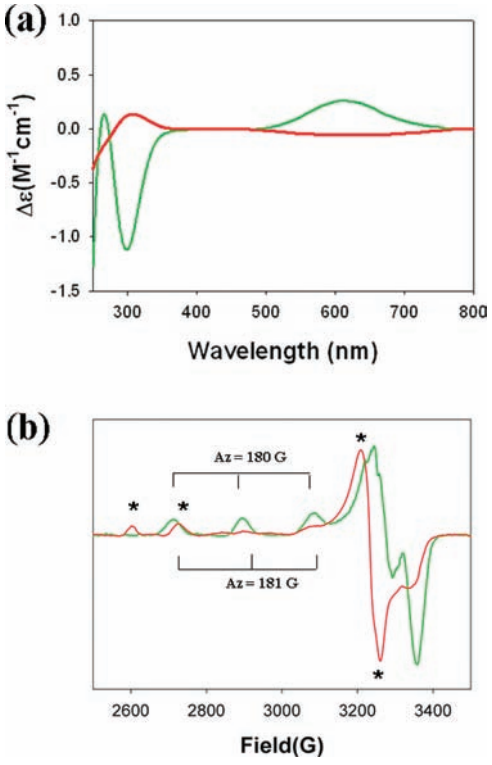

Figure 5. Role of Asp-2 residue in Cu(II) coordination to P1AS monitored by CD and EPR spectroscopy. (a) CD spectra of P1AS (green) and D2A-P1AS (red) complexes with 1 equiv of Cu(II). (b) X-band EPR spectra of P1AS (green) and D2A-P1AS (red) with 1 equiv of Cu(II). Asterisks in Figure b indicate signals associated to free Cu(II) in solution. All spectra were collected in buffer A at pH 6.5, under the conditions specified in the Experimental Section.

before DEPC treatment resulted also in the carbethoxylated species, indicating that when the carboxylate sidechain of Asp-2 is methylated, the DEPC-modified site in P1AS can not be protected by Cu(II). Since we have demonstrated previously that the sequence contained in P1AS coordinates specifically to Cu(II) and protects this site against DEPC modification (shown in Figures 4 d−f for comparative purposes), these findings suggest that Asp residue at position 2 might be a key residue for metal coordination to site 1.

To confirm the key role of Asp-2 in Cu(II) binding to P1AS, the variant D2A of the peptide P1AS (D2A-P1AS) was synthesized, and their Cu(II) binding features were characterized spectroscopically. Figure 5a shows the CD spectra of P1AS, and D2A-P1AS species with 1 equiv of Cu(II). Interestingly, the typical Cu(II) d-d transition band at 610 nm and the high intensity negative CT band at 300 nm are not detected in the CD spectra of D2A-P1AS with added Cu(II). Instead, an extremely weak positive band at 300 nm is detected for the D2A-P1AS-Cu(II) complex. These spectral changes likely reflect a different coordination environment for Cu(II) in the D2A-P1AS species. Moreover, the EPR spectrum of D2A-P1AS with 1 equiv of Cu(II) displays signals associated to free Cu(II) in solution (asterisks in Figure 5b), indicating a lower population of metal-complex formation upon the D2A substitution. The EPR spectrum also displays a minor species associated to peptide-bound Cu(II), with $g_z = 2.24$ and $A_z = 181\ \text{G} \equiv 189 \times 10^{-4}\ \text{cm}^{-1}$. Accordingly, ITC experiments on the D2A-P1AS peptide confirmed a significantly decreased binding affinity for Cu(II), with a dissociation constant $K_d = 11.80 \pm 1.12\ \mu\text{M}$ (Figure S3 in the Supporting Information). Altogether, these results indicate that Cu(II) binding to D2A-P1AS is less favorable than in the P1AS peptide and demonstrate that Asp-2 plays a key role in high affinity Cu(II) coordination to site 1. In particular, the Asp-2 residue binds directly to the metal ion and at the same time substantially increases the acidity of its amide proton exerting a double stabilizing effect on the formed metal complex.

Water Molecule Provides One Oxygen Ligand in Cu(II) Binding Site 1. To evaluate the participation of water molecules as equatorial ligands for Cu(II) bound to site 1 of AS, the peptide P1AS was titrated with Cu(II) in buffer A at pH 6.5 in either ^{16}O water or 60−70% ^{17}O enriched water. From the comparison of the X-Band EPR spectra of these samples (Figure 6), it becomes clear that the EPR spectrum of the ^{17}O enriched sample is significantly broader as compared to the ^{16}O sample. The line-width at half the maximal amplitude for the lowest field signal in the parallel region increases from 41 G for the ^{16}O sample to 54.5 G for the ^{17}O sample, that is, a broadening of 13.5 G. A similar broadening (of 12 G) can also be measured for the second parallel signal, as shown in the inset of Figure 6. Simulations of this broadening effect, considering 65% ^{17}O enrichment in the medium and one equatorial oxygen coordinated to the metal ion, lead to a hyperfine coupling constant for the ^{17}O of $13 \times 10^{-4}\ \text{cm}^{-1}$. The line broadening due to ^{17}O coupling is not significant for axial waters, while equatorial water ligands in

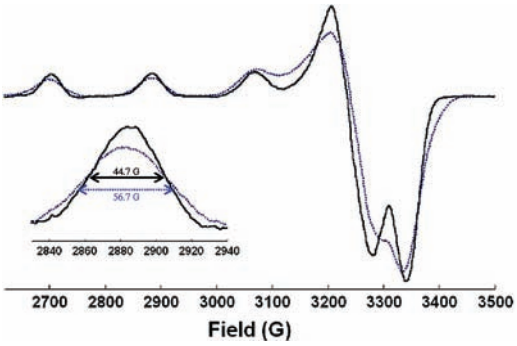

Figure 6. X-Band EPR spectra of P1AS with 0.8 equiv of Cu(II) in buffer A at pH 6.5, prepared with ^{16}O water (black) and ^{17}O enriched water (blue). Inset displays an enlargement of the second parallel signal, indicating the line-widths at half the maximal amplitude. Spectra were collected at 20 K under the conditions specified in the Experimental Section.

copper centers lead to superhyperfine coupling constants for ^{17}O in the order of 12 to 16 $\times$ 10^{-4} cm^{-1}, as reported for a Cu(II)-doped zinc Tutton's salt[79] and for a Cu(II)-acetylacetonate complex.[80] Similar ^{17}O superhyperfine coupling constants have been reported for copper proteins like the type-2 site in fungal laccase,[81] and for the active site in the ribulose-1,5-biphosphate carboxylase/oxygenase.[82] Thus, the ^{17}O superhyperfine coupling constant observed for the P1AS-Cu(II) complex is consistent with the presence of one water molecule coordinated in the equatorial position.

Structural Features of the Cu(II) Binding Site 1 in AS Determined by NMR Spectroscopy and Molecular Dynamics. 1. NMR Analysis. The details of Cu(II) binding to site 1 were explored at single-residue resolution by using 2D ^1H NMR spectroscopy. The electron spin relaxation from the paramagnetic Cu(II) ion results in the differential broadening of proton resonances linked to the paramagnetic center by through-bond or through-space interactions, providing the means for mapping the metal binding site in the peptide and elucidating the structure of the Cu(II)-complex based on paramagnetic NMR distance restraints.[55]

The NMR investigation of the P1AS-Cu(II) complex was performed on 600 μM peptide samples at pH 6.5. The addition of copper to P1AS caused selective proton line broadening and proton paramagnetic relaxation enhancement (R_{1p}), as reported in Figure 7a, b. Analysis of the ^1H-^1H TOCSY spectra shows that the most affected aminoacids are Met-1 and Asp-2. After the addition of Cu(II), the Hα proton of Met-1 completely disappears and the Hβ and Hγ protons are less intense. Also the Hα and Hβ protons of Asp-2 showed a decreased intensity, indicating their proximity to the metal ion. On the contrary, the analysis of the proton relaxation rate enhancements belonging to residues Val-3, Phe-4, Met-5, and Lys-6 revealed no changes, indicating that these protons are distant from the metal binding site.

Analysis of Cu(II) binding to the D2A-P1AS peptide was also performed by NMR spectroscopy (Figures 7c,d). As in the case of P1AS, significant changes in cross peak intensities occurred in the N-terminal region of the peptide, with the strongest broadening effects corresponding to proton resonances of Met-1, Ala-2, and Val-3. Interestingly, the paramagnetic effects measured on D2A-P1AS were more pronounced and generalized than in the P1AS species, as reflected by the magnitude of the proton relaxation rate enhancements and the larger range of affected resonances (Figure 7d). On the contrary, a noticeable difference was observed between metal binding capabilities of both peptides in the order P1AS $\gg$ D2A-P1AS, as determined by ITC. These discrepancies can be reconciled by comparing the metal binding features with the residence lifetime (τ_M) of the metal ion in the coordination sphere of each peptide. An estimation of this parameter can be done assuming a global correlation time (τ_C) of 0.4 ns and considering that binding to the N-terminal amino group, as pointed out by our previous results, brings the Met-1 Hα at distances from Cu(II) in the range 0.23$-$0.40 nm.[35] The theoretical values of R_{1b} consistent with these distances can be therefore calculated from eq 3 and inserted in eq 2 to obtain τ_M values. By using this approach, τ_M values $\leq$5 ms and $\geq$35 ms were estimated for the metal complexes of D2A-P1AS and P1AS, respectively. Since a longer residence time obviously identifies a stronger metal$-$ligand association, these results correlate well with the affinity order determined for the copper complexes P1AS $\gg$ D2A-P1AS. On the other hand, these results indicate that the residence lifetime of the metal at the P1AS binding site contributes significantly to the observed relaxation rates, thus justifying the relative small paramagnetic effects experienced by the proton resonances on the P1AS-Cu(II) complex (Figure 7b). In such a situation, the closer a proton to the paramagnetic ion the larger R_{1b} is, and therefore, the more important the contribution of τ_M to the proton relaxation rate enhancements (R_{1p}) becomes.[55] Thus, the paramagnetic effects may become almost exclusively determined by the exchange rate of the binding motif from the copper coordination sphere, and the proton-metal distances cannot be measurable with precision. Accordingly, although the NMR results shown here support clearly the involvement of Met-1 and Asp-2 residues in Cu(II) coordination, structural determination of the P1AS-Cu(II) complex based on paramagnetic NMR distance restraints is not feasible.

Further information of Cu(II) binding to P1AS was gained from monitoring the paramagnetic effects induced by the metal ion on the ^{13}C NMR spectra. The widespread dispersion in chemical shifts of the different carbon atoms in the aminoacid residues of P1AS provide excellent probes to study the coordination properties of the P1AS-Cu(II) complex. The ^1H and ^{13}C NMR chemical shifts assignment of P1AS resonances is shown in Table S3 in the Supporting Information. As shown in Figures 8 a$-$c, the Met-1 Cα and CO and the Asp-2 Cβ and COO^- resonances vanished out upon addition of the metal ion. Resonances corresponding to Asp-2 Cα and Met-1 Cβ and Cγ were also affected, although to a lesser effect, whereas no changes were observed on signals belonging to the ^{3}VFMK^6 segment. The combined use of ^1H-^{13}C

(79) Getz, D.; Silver, B. L. *J. Chem. Phys.* **1974**, *61*, 630–637.
(80) Vänngård, T. In *Biological Applications of Electron Spin Resonance*; Swartz, H. M., Bolton, J. R., Borg, D. C., Eds.; Wiley-Interscience: New York, 1972.
(81) Brändén, R.; Deinum, J. *FEBS Lett.* **1977**, *73*, 144–146.
(82) Styring, S.; Brändén, R. *Biochemistry* **1985**, *24*, 6011–6019.

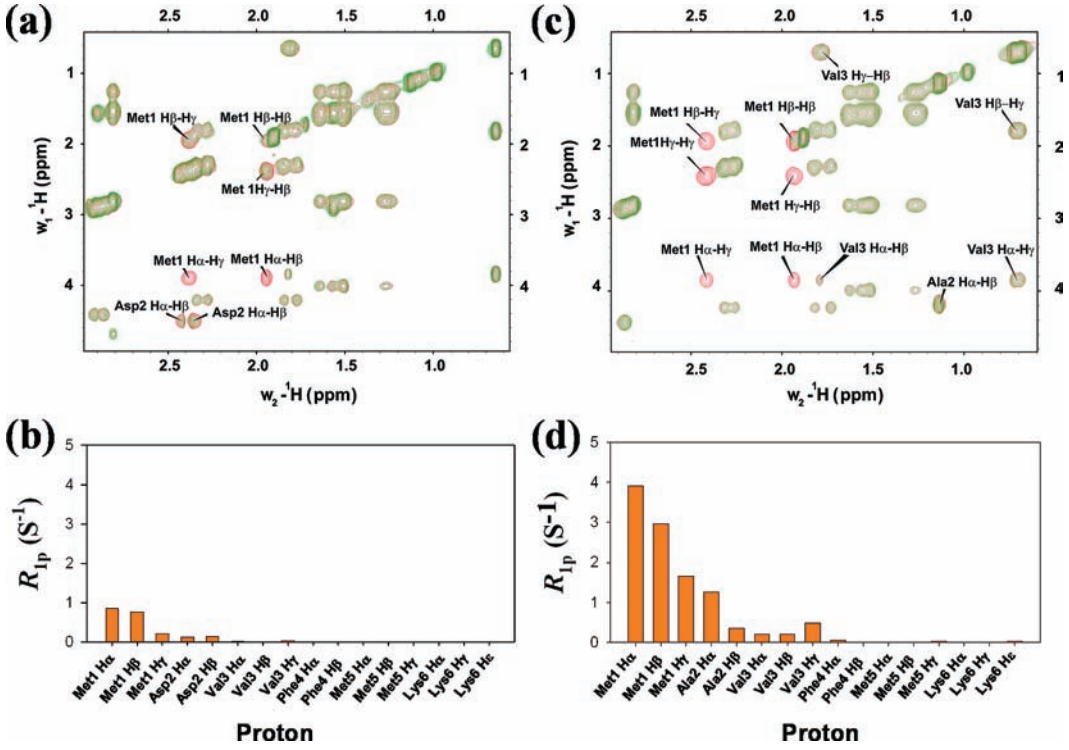

Figure 7. ^{1}H-^{1}H TOSCY and proton paramagnetic relaxation contribution (R_{1p}) of aliphatic resonances in P1AS (a, b) and D2A-P1AS (c, d). Spectra were collected in deuterated buffer A at pH 6.5 and 15 °C. Metal to protein ratios of 1:35 and 1:50 were used for the P1AS and D2A-P1AS species, respectively. Overlaid spectra in red and green correspond to the free and Cu(II) complexed species, respectively. Amino acid residues broadened significantly or beyond detection are identified.

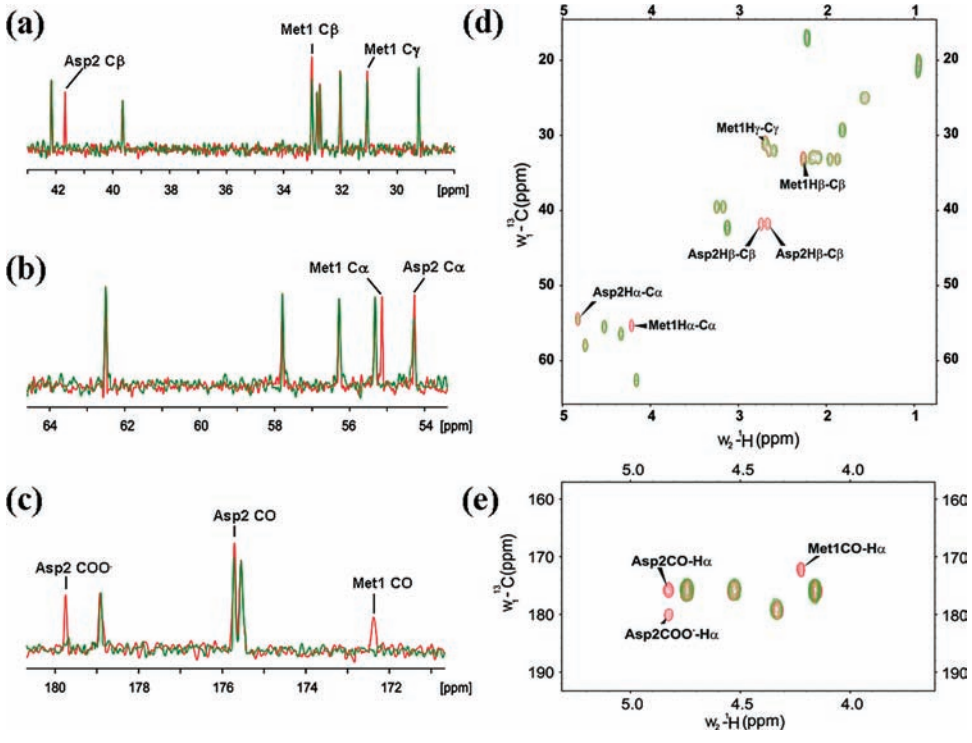

Figure 8. ^{13}C NMR analysis of Cu(II) binding to P1AS. Overlaid 1D ^{13}C NMR spectra of P1AS in the absence (red) and presence (green) of Cu(II) in the characteristic Cβ, Cγ (a), Cα (b), and CO spectral regions (c). Panel d shows the overlaid ^{1}H-^{13}C HSQC spectra of P1AS in the absence (red) and presence (green) of Cu(II) in the aliphatic spectral region. Panel e shows the overlaid ^{1}H-^{13}C HMBC of P1AS in the absence (red) and presence (green) of Cu(II) in the CO-Hα spectral region. Amino acid residues broadened significantly or beyond detection are identified. Spectra were collected using a 2.5 mM peptide concentration and 1:15 metal/peptide ratio in D_2O at pH 6.5 and 15 °C.

HSQC and HMBC experiments allowed us to assign unambiguously the resonance corresponding to the CO of Asp-2 (Figure 8 d and e), confirming that the perturbation observed on the intensities of the overlapped resonances at

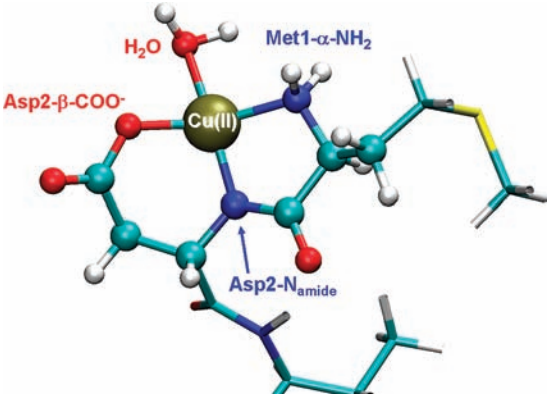

Figure 9. Structure of one of the AS-Cu(II) conformers, as obtained by QM/MM simulation.

Table 1. Average Values of Selected Bond Lengths and Angles for the AS-Cu(II) Site 1 Complex Calculated over 18 QM/MM MD Trajectories

Cu(II)-ligand bond lengths and angles from the AS-Cu(II) site 1 complex		mean bond length and angle values reported for other Cu(II) complexes[a]
$Cu(II)-NH_2$	2.056 ± 0.018 Å	2.00 Å
$Cu(II)-N^-_{amide}$	1.924 ± 0.016 Å	1.92 Å
$Cu(II)-O^-_{carboxylate}$	2.009 ± 0.019 Å	1.98 Å
$Cu(II)-O_{water}$	2.089 ± 0.024 Å	1.97 Å
$O_{carboxylate}-Cu(II)-NH_2$	164.3 ± 1.8°	167°
$O_{water}-Cu(II)-N^-_{amide}$	167.5 ± 1.6°	166°
$N^-_{amide}-Cu(II)-NH_2$	83.5 ± 0.7°	83.5°
$O_{water}-Cu(II)-O^-_{carboxylate}$	87.6 ± 1.4°	84.0°

[a] Mean bond length and angle values were obtained from the crystal structures of peptide-Cu(II) complexes in tetragonal, square planar, or octahedral coordination geometries.[83]

175.8 ppm in the 1D ^{13}C NMR spectrum of the P1AS-Cu(II) complex is due to the paramagnetic influence of Cu(II) on that signal.

Altogether, these observations confirm the unique involvement of Met-1 and Asp-2 in Cu(II) coordination to P1AS and give further support to the role of the carboxylate side chain (COO^-) of Asp-2 as metal anchoring group.

2. MD Analysis. A structural model for the Cu(II) complex at site 1 of AS was built based on 18 representative AS structures identified previously.[57] According to our experimental results, the donor atoms of the metal ion were the Met-1 N-terminal and Asp-2 backbone nitrogens, Asp-2 carboxylate side-chain, and a water molecule. The complexes underwent classical MD simulations and subsequently a QM/MM MD at 300 K.

The classical MD allowed the relaxation of the protein frame in the presence of the metal ion. The QM/MM calculations allowed the structure of the copper coordination sphere to relax. One of the resulting WTAS-Cu(II) conformers, as simulated by QM/MM MD, is shown in Figure 9. The average structural parameters, obtained as a weighted average over every representative conformer, indicate a distorted tetragonal coordination geometry (Table 1 and Table S4 in the Supporting Information).[83]

Addressing the Role of Cu(II) Binding Site 1 on the Metal-Mediated AS Aggregation. To ascertain the binding-aggregation features of the AS-Cu(II) complex formed at site 1, we studied the effect of the metal ion on the aggregation rate of H50A AS and the C-terminal truncated variants 1−108 AS and H50A 1−108 AS. These variants represent a useful model system to understand the mechanism by which copper induces AS aggregation, in particular, whether specific binding of Cu(II) to site 1 is sufficient to trigger amyloid formation. The time course of aggregation of AS species in the absence and presence of 1 equiv of Cu(II) was monitored by 1D ^1H NMR (Figure 10a). Under these conditions, only the metal binding site 1 is significantly occupied. The characteristic $t_{1/2}$ for aggregation of WT and H50A AS proteins were reduced from ∼30 h to ∼20 h in the presence of 1 equiv of Cu(II) (Figure 10b and Figure S4a in the Supporting Information). The fact that the $t_{1/2}$ of aggregation of the H50A mutant is comparable to that of the wild-type protein (∼30 h) allows us to discard a critical role for His-50 in the fibrillation pathway of AS, whereas the similar effects of Cu(II) on the aggregation of WT and H50A species indicate that the critical step in copper-mediated AS aggregation is the formation of the AS-Cu(II) complex at site 1. Comparable results were independently obtained by the standard thioflavin T (ThT) fluorescence assay (Figure S5 a−c in the Supporting Information).

As reported previously, the aggregation kinetics for the C-terminal truncated species (1−108 AS) were faster compared to that of the wild-type protein, supporting a

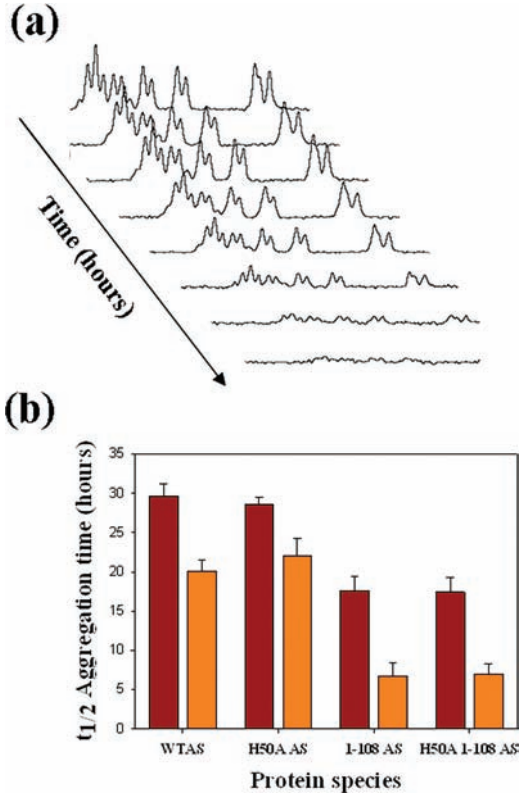

Figure 10. Aggregation kinetics of WTAS and its point and C-terminal truncation mutants H50A, 1−108 AS and 1−108 H50A AS, determined by NMR spectroscopy. (a) Representative set of 1D ^1H NMR spectra of WTAS as a function of time. Monomer consumption was quantified by integration of the NMR signals and fit as described in the Experimental Section. (b) Values of the $t_{1/2}$ of aggregation for the different proteins studied, in the absence (dark red) and presence of 1 equiv of Cu(II) (orange). All experiments were performed on 100 μM protein samples dissolved in buffer A at pH 6.5 and 37 °C.

(83) Freeman, H. C. *Adv. Protein Chem.* **1967**, *22*, 257–424.

role for the C-terminus in modulating AS aggregation propensity (Figure 10b and Figure S4b in the Supporting Information).[9] When 1 equiv of Cu(II) was added to the 1−108 and H50A 1−108 species the aggregation $t_{1/2}$ values were reduced from ∼18 h to ∼6 h (Figure 10b and Figure S4b in the Supporting Information) for both species, demonstrating conclusively that the acceleration of AS aggregation induced by Cu(II) is driven by its specific binding to site 1.

Conclusions

In this work, we report the high-resolution structural characterization of the high-affinity Cu(II) binding site of AS and analyze the consequences of this interaction on the aggregation kinetics of the protein. We provide direct experimental evidence and demonstrate conclusively that the source of nitrogens in the N2O2 ligand set comes from the α-amino group of Met-1 and the amide backbone of Asp-2, whereas the oxygen ligands are provided by the carboxylate side-chain (COO^-) of Asp-2 and a water molecule that coordinates the metal ion in an equatorial position. The structural parameters are characteristic of a Cu(II) coordination in a type II distorted tetragonal arrangement. Moreover, specific Cu(II) binding to site 1 was found to be the critical step in the metal-mediated AS fibrillation process.

New insights into the structural and mechanistic basis behind copper-mediated AS aggregation are implied by these findings. Unlike the Aβ peptide and prion protein, that were previously shown to aggregate more readily following the formation of histidine Cu(II) complexes, the presence of His-50 in AS sequence does not influence the aggregation process triggered by copper, arguing against an active role for this residue in the structural and biological events involved in the mechanism of copper-mediated AS aggregation. The presence of copper-coordinating histidine residues at different locations of the Aβ and prion sequences, compared with the sole His-50 in AS, seems to be a key difference that influences significantly the aggregation process mediated by the presence of Cu(II) in these proteins.

Interestingly, our results also indicate that the oligomerization process mediated by Cu(II) binding to site 1 of AS is more efficiently triggered on the C-terminal truncated species. Since the C-terminal region plays an inhibitory role on the aggregation propensity of AS, an appealing hypothesis is that Cu(II) binding to site 1 might perturb transient long-range interactions between the N- and C-terminal regions in the wild-type protein. The lack of these tertiary interactions in the C-terminal truncated species would result in an acceleration of the aggregation rates in the presence of copper compared to the wild type protein. The differences found between the enthalpic and entropic contributions measured for the Cu(II) complexes in the peptide and the full length protein species might be reflecting these conformational changes. Accordingly, formation of a AS-Cu(II) complex at site 1 and destabilization of long-range interactions between the N- and C-terminus might represent the critical step in the early stage of the metal-mediated fibrillation of the protein.

As previously reported, AS is highly susceptible to metal-catalyzed oxidation,[84−86]a reaction that involves the reduction of Cu(II) by a suitable electron donor and the conversion of molecular oxygen into reactive oxygen species (ROS). Indeed, metal-enhanced AS aggregation associated to the occurrence of Cu(I)/dioxygen chemistry was reported recently,[87] although detailed knowledge of the structural and binding features of Cu(I) to AS remains unknown. The fact that metal-catalyzed oxidation of proteins is a highly selective, site-specific process that occurs primarily at protein sites with transition metal-binding capacity gives further support to this hypothesis. At this juncture, one can thus hypothesize that copper binding to the N-terminus of AS might render the protein a relative easy target for oxidative damage and that the ensuing damage might lead to a cascade of structural alterations promoting the generation of a pool of AS molecules more prone to aggregate.

That AS binds Cu(II) with an affinity in the submicromolar range and that this specific interaction efficiently promotes AS aggregation support the notion of PD as a metal-associated neurodegenerative disorder. The high-resolution structural information emerging from this work constitutes a key step toward the understanding of the mechanistic basis behind the Cu(II)-mediated AS aggregation in Parkinson's disease.

Acknowledgment. C.O.F. thanks ANPCyT, Fundación Antorchas, CONICET, Max Planck Society, and the Alexander von Humboldt Foundation for financial support. C. O.F. is the head of a Partner Group of the Max Planck Institute for Biophysical Chemistry (Göttingen). A.B. is recipient of a fellowship from CONICET in Argentina. M.Z. is supported by a DFG Heisenberg scholarship (ZW 71/2-1 and 3-1). E.E.R. is recipient of a fellowship from CONACYT in Mexico. L.Q. thanks CONACYT (J4878Q-1) and ICyTDF (PIFUTP08-161) for financial support. The authors would like to thank Prof. Martha Sosa and Dr. Alejandro Solano for allowing access to a Bruker ELEXSYS E500 EPR system, which was purchased with funds from CONACYT (41128Q). The Bruker Avance II 600 MHz NMR spectrometer used in this work was purchased with funds from ANPCyT (PME2003-2006) and CONICET. Computer resources used for the theoretical calculations from "Progetti Supercalcolo 2008" at CINECA are gratefully acknowledged.

Supporting Information Available: Technical details of MD simulations; tables containing parameters for EPR spectra simulation, fragments generated by CID MS/MS, NMR chemical shifts of P1AS, and percentage of AS conformers used for MD; and Figures showing EPR spectra, MALDI-MS, ITC, and aggregation data of peptides and proteins used in this work. This material is available free of charge via the Internet at http://pubs.acs.org.

(84) Kowalik-Jankowska, T.; Rajewska, A.; Jankowska, E.; Wisniewska, K.; Grzonka, Z. *J. Inorg. Biochem.* **2006**, *100*, 1623–1631.
(85) Paik, S. R.; Shin, H. J.; Lee, J. H. *Arch. Biochem. Biophys.* **2000**, *378*, 269–277.
(86) Yamin, G.; Glaser, C. B.; Uversky, V. N.; Fink, A. L. *J. Biol. Chem.* **2003**, *278*, 27630–27635.
(87) Lucas, H. R.; Debeer, S.; Hong, M. S.; Lee, J. C. *J. Am. Chem. Soc.* **2010**, *132*, 6636–6637.